THE JOURNAL OF
PHYSICAL CHEMISTRY C

Article

pubs.acs.org/JPCC

Rate Theory of Ion Pairing at the Water Liquid−Vapor Interface

Liem X. Dang* and Gregory K. Schenter

Physical Sciences Division, Pacific Northwest National Laboratory, Richland, Washington 93352, United States

Collin D. Wick

College of Engineering and Science, Louisiana Tech University, Ruston, Louisiana 71272, United States

ABSTRACT: There is overwhelming evidence that certain ions are present near the liquid−vapor interface of aqueous salt solutions. Despite their importance in many chemical reactive phenomena, how ion−ion interactions are affected by interfaces and their influence on kinetic processes is not well understood. We carried out molecular simulations to examine the thermodynamics and kinetics of small alkali halide ions in the bulk and near the water liquid−vapor interface. We calculated dissociation rates using classical transition-state theory and corrected them with transmission coefficients determined by the reactive flux method and Grote−Hynes theory. Our results show that in addition to affecting the free energy of ions in solution, the interfacial environments significantly influence the kinetics of ion pairing. Results on the relaxation time obtained using the reactive flux method and Grote−Hynes theory present an unequivocal picture that the interface suppresses ion dissociation.

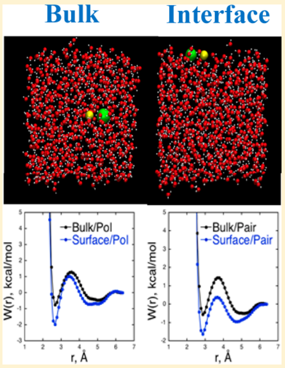

1. INTRODUCTION

The thermodynamics and kinetics of ion pairings at interfaces are fundamental processes encountered in a wide range of physical and chemical systems.[1−3] The structure and stability of large molecules and membranes depend on the interfacial distribution of ions and counterions. Moreover, the ion transport mechanism can be an important factor in atmospheric processes, such as molecular uptake at the liquid−air interface.[4] It is also of importance in environmental problems, such as the interaction of contaminated organic solvents in groundwater and separation chemistry performed in binary solvent systems.[5]

Considerable progress has been made in understanding the equilibrium and dynamical properties of ion pairings at liquid interfaces. This includes the work of Schweighofer and Benjamin on the thermodynamics and dynamics of NaCl dissociation at the water−1,2-dichloroethane liquid−liquid interface using a variety of statistical mechanical tools, such as the continuum electrostatic model, molecular dynamics free energy calculations, and nonequilibrium dynamic trajectory calculations.[6] Their results indicated that the dissociation of the ion pair at the interface involves a simultaneous transfer of both ions into the aqueous side of the interface. In addition, they found that faster transfer of sodium ions (Na^+) than chloride ions (Cl^-) influences the length of time the ion pair spends at the interface. Wick reported a study on the NaCl dissociation rate both in the aqueous bulk and at the air−water interface using the transition path sampling formalism with a polarizable force field. A dissociation rate that was considerably slower at the interface than that in the bulk was found.[7] Garde and co-workers used molecular simulations to show that the potentials of mean force (PMFs) between small ions change character dramatically near the water vapor−liquid interface. Specifically, the water-mediated attraction between oppositely charged ions is enhanced relative to that in bulk water. Moreover, they showed that the thermodynamics of ion association are governed by a delicate balance of ion hydration, interfacial tension, and restriction of capillary fluctuations at the interface, leading to nonintuitive phenomena such as water-mediated, like-charge attraction.[8] Interfacial ion pairing has recently been investigated via second-harmonic generation experiments by Saykally and co-workers using different kinetic models.[9] They provided insight into how ion pairing influenced anion behavior at the interface, finding that unusually strong surface adsorption is possible at low concentrations. X-ray reflectivity experiments reported by Schlossman and co-workers have shown that the enhancement of ion density near the interface coupled with the effect of capillary waves may lead to layering of erbium chloride at the air−water interface.[10] Allen and co-workers carried out surface-sensitive conventional vibrational sum frequency generation and heterodyne-detected spectroscopy studies on the small alkali halide salt at the water liquid−vapor interface. Among other findings, they found that in the conventional VSFG spectra LiCl and NH_4Cl significantly perturb the hydrogen-bonding network of water. In addition, the direction of the electric field suggests that Cl^- ions are always located above the counter cations, even in the case of NH_4Cl salt solution.[11]

The main goal of our work, in addition to studying ion−ion PMFs, is to provide detailed kinetic properties of ion pairings at

Received: March 8, 2017
Revised: April 19, 2017
Published: April 24, 2017

DOI: 10.1021/acs.jpcc.7b02223
J. Phys. Chem. C 2017, 121, 10018−10026

the liquid−vapor interface of water using a variety of rate theory approaches. Moreover, we will determine how the inclusion of polarizable interactions influences the differences that arise at the interface versus bulk. Subsequently, our studies will be expanded to other interfaces, such as liquid−liquid interfaces. Knowledge of free energy profiles and rate theory evaluations is important for understanding a wide range of physical and chemical phenomena for ion solvation and pairing. These also provide a challenging test of the accuracy of the predictive information derived from force field models. Our work is distinguished from earlier contributions by the methodology and the extent to which we have exploited rate theory approaches including classical transition-state theory (TST),[12] the reactive flux (RF) formalism,[13] and Grote−Hynes (GH) theory.[14] In addition, (1) polarization effects are explicitly included in the potential models and compared with nonpolarizable models, (2) solvent response at the interface and in the bulk are evaluated using a variety of classical rate theory approaches, and (3) the dissociation lifetimes for the ion pair are computed and compared for different potential models and theories. The remainder of this paper is organized as follows. In section 2, we describe the potential models and simulation methods used. Results and discussion are presented in section 3, and our conclusions are provided in section 4.

2. POTENTIAL MODELS, SIMULATIONS, AND METHODS

For water−water interactions, we employed the Dang−Chang polarizable water model,[15] and ion parameters for Na^+ and Cl^- were taken from our previous work.[16] Our Dang−Chang model provides a reasonable surface tension value of 61 dyn/cm and a computed surface potential value of −0.50 ± 0.01 V, which lies within the experimental range of −1.1 to 0.5 ± 0.01 V. These computed values are also compared well with the best potential models available in the literature. Our Dang−Chang model has also been used to study the interfacial thermodynamic properties of NaCl solutions, and good results were obtained from these studies. In Figure 1, we show a schematic description of the $NaCl-H_2O$ systems under study. In this figure, both Cl^- and Na^+ ions are located in the bulk in the left panel, and both Cl^- and Na^+ are located at the Gibbs dividing surface in the right panel. Equation 1 was used to calculate the ion−ion mean force as an average over the different solvent configurations[17]

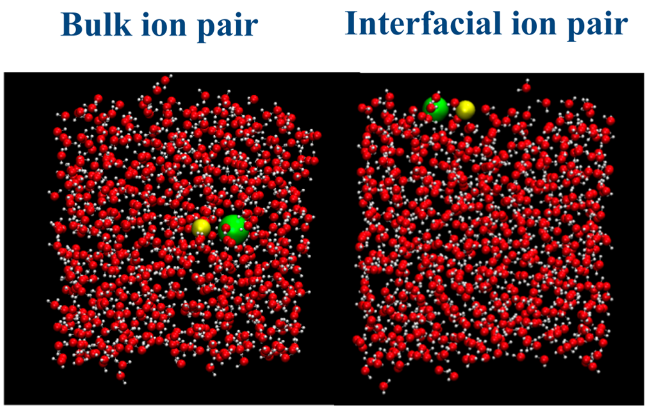

Bulk ion pair

Interfacial ion pair

Figure 1. Schematic description of the $NaCl-H_2O$ system under study. The left panel is for the ion pair in the bulk region, and the right panel is for the ion pair at the Gibbs dividing surface. The reduced amount of solute−solvent coupling at the surface is evident from the figure.

$$F(r) = \frac{1}{2}\langle \vec{r}_u \cdot (\vec{F}_A - \vec{F}_B)\rangle \qquad (1)$$

In this expression, F_A and F_B are the forces acting on the ions. The term $\vec{r}_u$, which is a unit vector along the A−B direction, is defined as

$$\vec{r}_u = \vec{r}_{AB}/|r_A - r_B| \qquad (2)$$

The PMF, $W(r)$, is calculated as

$$W(r) = -\int_{r_o}^{r_s} \langle F(r)\rangle \, dr \qquad (3)$$

We evaluated PMFs as a function of the separation in Na^+-Cl^-, with the distance between them incremented by 0.1 Å. At each separation, the average $F(r)$ was determined from a 2 ns simulation time, preceded by a 500 ps equilibration period. The uncertainties on the PMFs were ±0.05 kcal/mol, as estimated by determining the force averaged over four equally spaced time windows during the production. The systems investigated consisted of one Na^+-Cl^- ion pair in 700 water molecules. The position of the ion pair with respect the system center of mass was fixed by removing the forces and velocities acting on their center masses in the direction perpendicular to the interface. All simulations were performed using a modified version of Amber9.[18] We employed the *NVT* ensemble at 300 K and the Berendsen thermostat[19] to control the temperature with periodic boundary conditions applied in all three directions with a time step of 2 fs. The Ewald summation technique was used to handle long-range electrostatic interactions,[20] and the SHAKE[21] algorithm was used to fix the internal water geometry.

3. RESULTS AND DISCUSSIONS

3.A. Kinetics of Interfacial Ion Pairing with Polarizable Models. We begin this section by presenting results on the kinetic properties of NaCl ion pair formation at the interface and in the bulk and then continue with the rate theory results determined using the RF and GH methods. We end this section with a comparison of results obtained using the different rate theory methods, along with a description of their solvation structures. Figure 2 shows the computed PMF plots as a function of NaCl separation at the interface and in the bulk for the polarizable model. Although the shapes for both of the PMFs are quite similar, the details of the barriers are different, which may result in dissimilarities in the kinetics of ion paring. From Figure 2, it is clear that the PMF at the interface has a deeper minimum at the contact ion pair and a larger barrier height to dissociate compared to the corresponding bulk PMF results. This demonstrates that the interfacial ion pair is more strongly associated at the interface, which can be attributed to the rearrangement of the interfacial water hydrogen networks to accommodate the ion pair at the interface. Moreover, it is well-known that Cl^- has a larger induced dipole at the interface,[22] which should further strengthen NaCl pairing at the interface. Another interesting aspect of the PMF is that the solvent-separated ion pair probability (its free energy is lower near 4.5 Å) is slightly enhanced at the interface with respect to the bulk. Overall, this shows that ions are more likely to not just be paired but to be paired within their first two solvation shells near the interface. The free energy barriers for the ion pair

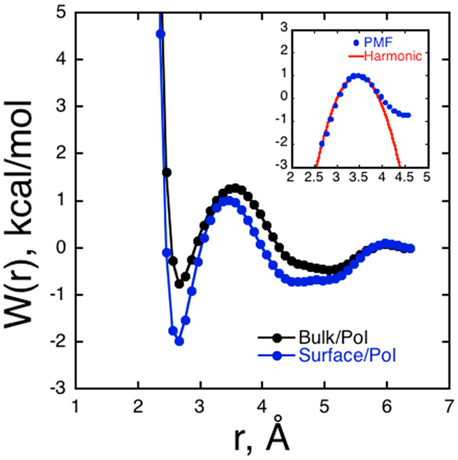

Figure 2. Computed PMFs for the NaCl ion pair in the bulk and at the interface. This is consistent with the fact that the surface is less effective at screening stabilization of the ion pair (polarizable model). The inset shows the invert parabolic fits (red color) to the barrier for the interfacial ion pair.

dissociation are found to be about 3.0 and 2.0 kcal/mol for the interfacial and bulk ion pairs, respectively.

For a given PMF, the rate constant for the dissociation process can be computed using TST as follows[12]

$$k^{\mathrm{TST}} = \sqrt{\frac{k_{\mathrm{b}}T}{2\pi\mu}}\,\frac{(r^*)^2 \mathrm{e}^{-\beta W(r^*)}}{\int_0^{r^*} r^2 \mathrm{e}^{-\beta W(r)}\,\mathrm{d}r} \tag{4}$$

where r^* is defined as the position of the barrier top, μ is the ion−water reduced mass, k_{b} is the Boltzmann constant, and T is the temperature. The computed rate constants from the PMFs using TST are determined to be 0.28 and 0.07 ps^{-1} for the bulk and interface, respectively. These results show that the 1.0 kcal/mol higher barrier for dissociation at the interface has a major effect on the dissociation rate. These results are summarized in Table 1.

Table 1. Free Energy Barrier for Dissociation (PMF) and Rate Theory Results, Polarizable Model

	PMF/kcal/mol	k^{TST}/ps	κ_{RF}	κ_{GH}
bulk	2.00	0.28	0.14	0.18
interface	2.80	0.07	0.25	0.33

The RF method and GH theory approaches provide a transmission coefficient, κ, to correct the TST. In the RF method, the transmission coefficient, κ_{RF}, is extracted from the plateau value of the time-dependent transmission coefficient as calculated using eq 5

$$\kappa_{\mathrm{RF}}(t) = \frac{\langle (v\cdot\hat{r})\delta(r - r^*)\theta(r(t) - r^*)\rangle_{\mathrm{c}}}{\langle (v\cdot\hat{r})\delta(r - r^*)\theta(v\cdot\hat{r})\rangle_{\mathrm{c}}} \tag{5}$$

The term $v\cdot\hat{r}$ represents the initial ion−ion velocity, and $\theta(v\cdot\hat{r})$ is the Heaviside function to account for only positive velocities. The subscript c means that the initial configurations have been generated in the constrained reaction coordinate ensemble. We performed the RF method using the *NVE* ensemble with the initial configurations generated from the *NVT* ensemble. Hence, our computed transmission coefficients are not affected adversely by thermostatting. In Figure 3, we present the computed time-dependent $\kappa(t)$ for both ion pair locations using the RF method. The transmission coefficients, κ_{RF}, are 0.14 and 0.25. We observed that the plateaus of the transmission coefficient curves are very flat after 1.5 ps, and we also noticed that the transmission coefficients decrease from the interface to the bulk. Our results show that in addition to affecting the free energy of solvation, moving ion pairs from the bulk to the surface should significantly influence the kinetics of ion pairing. In Table 1, we present the rate constant results obtained using TST and the transmission coefficient obtained by the RF method, κ_{RF}. The product of κ_{RF} and k^{TST} gives the corrected rate constant. Taking the inverse of the rate constant gives the relaxation time for the reaction. We found that the relaxation times increased from 26 to 57 ps when the ion pair was at the interface in comparison to the bulk. These results confirm that the interface has a significant impact on the kinetics of ion pairing for models with polarizable interactions.

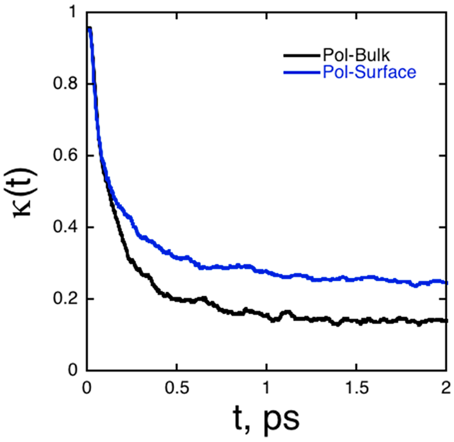

Figure 3. Computed $\kappa(t)$ using the RF method for the NaCl ion pair in the bulk and at the Gibbs dividing surface. The enhancement of the rate for the surface is due to reduced coupling to the solvent. The time scale of the response appears to be the same (polarizable model).

We were also interested in using GH theory to calculate a transmission coefficient, κ_{GH}, to compare with the RF results. To accomplish this task, we computed the friction kernel using the trajectories at the PMF barrier

$$\zeta(t) = \frac{1}{\mu k_{\mathrm{b}}T}\langle R(t, r^*)\cdot R(0, r^*)\rangle \tag{6}$$

$$R(t, r) = F(t, r) - \langle F(t, r)\rangle \tag{7}$$

The term r^* is the position of the barrier maximum, μ is the reduced mass, k_{b} is the Boltzmann constant, and T is the temperature. The transmission coefficient from GH theory, κ_{GH}, can be expressed as[17]

$$\kappa_{\mathrm{GH}} = \left(\kappa_{\mathrm{GH}} + \int_0^{\infty} \mathrm{d}t\,\frac{\zeta(t)}{\omega_{\mathrm{b}}}\mathrm{e}^{-\omega_{\mathrm{b}}\kappa_{\mathrm{GH}}t}\right)^{-1} \tag{8}$$

The GH theory transmission coefficient involves the frequency component of the time-dependent friction coefficient, $\zeta(t)$, at the Laplace frequency, $\omega_{\mathrm{b}}\kappa_{\mathrm{GH}}$, relevant in the barrier region. The term ω_{b} is the barrier frequency obtained by fitting the PMF in the barrier region to an inverted parabola. As for the case of GH theory, we carried out multiple 2 ns, *NVT* ensemble simulations with different initial configurations. The final kernel friction was obtained from the average of these runs. In Figure 4, we show plots of

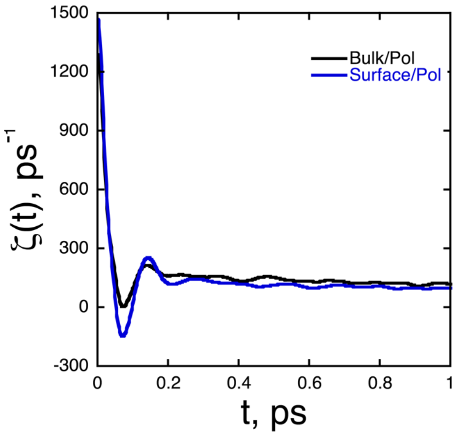

Figure 4. Computed friction kernel, $\zeta(t)$, used in both GH theory and GLE dynamics for the NaCl ion pair in the bulk and at the Gibbs dividing surface. The ringing at short time is less damped for the surface case, consistent with reduced coupling with the solvent (polarizable model).

unnormalized, time-dependent friction kernels of the ion pair at the interface and in bulk water for comparison. In all cases, there are two distinct decay time scales that show first an initial rapid decay, lasting for about 0.1 ps, and then a longer time decay that lasts for a few picoseconds. The oscillating characteristic of $\zeta(t)$ is reflected in the magnitude of the barrier heights shown in the computed PMFs. For instance, the larger barrier heights correspond to the deeper well-depth in the $\zeta(t)$. We calculated a barrier frequency, ω_b, of 76.4−88.1 cm^{-1} for the bulk and interfacial ion pairs, respectively. The computed transmission coefficients using GH theory are given in Table 2. Using the rate constants from TST, correcting them with the transmission coefficient, and taking their inverse, the relaxation time can be calculated. The bulk and interfacial ion pairs had relaxation times of 18 and 39 ps, respectively. These are somewhat lower than the times calculated from the RF method, but they are consistent. Results for the relaxation times obtained from the RF method and GH theory unequivocally show that the interface suppresses ion dissociation.

Table 2. Free Energy Barrier for Dissociation (PMF) and Rate Theory Results, Nonpolarizable Model

	PMF/kcal/mol	k^{TST}/ps	κ_{RF}	κ_{GH}
bulk	2.00	0.23	0.17	0.16
interface	2.00	0.27	0.18	0.28

3.B. Kinetics of Interfacial Ion Pairing with Nonpolarizable Models in Comparison with Polarizable Models. To better understand the specific role that polarizability plays in dissociation kinetics, we carried out similar calculations using nonpolarizable models. For these calculations, we employed the Tip4P-Ew water model, and the ion parameters were derived to reproduce many experimental properties.[23] In Figure 5, we present the computed PMF plots for the interfacial ion pair and the bulk ion pair for the nonpolarizable models. Similar to the polarizable models, there is a deeper free energy minimum at the contact ion pair (around $r = 3$ Å). However, the barrier heights for dissociation are very similar at the interface and the bulk (i.e., about 2.0 kcal/mol). This result is in contrast with the results obtained from the corresponding PMF that used polarizable models mentioned above. Also, the free energy at the solvent-separated ion pair is significantly different at the interface than in the bulk, with the surface results being more than 0.5 kcal/mol more negative in free energy at a distance of around 4.8 Å than the bulk value. This is greater than the difference observed in Figure 2 for the polarizable model. Overall, it seems that the interface stabilizes the contact ion pair for both models, while the nonpolarizable model provides slightly less, but still a significant degree of, stabilization of the solvent-separated ion pair due to the interface.

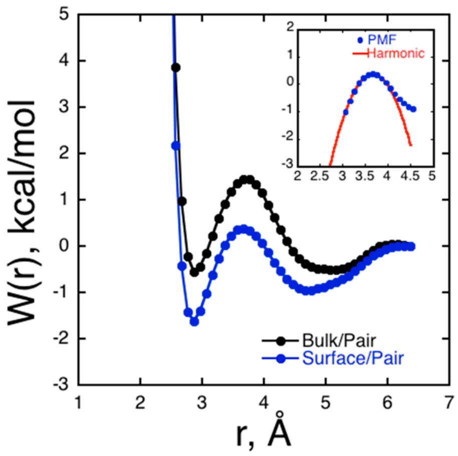

Figure 5. Computed PMFs for the NaCl ion pair in the bulk and at the Gibbs dividing surface using the nonpolarizable model. The qualitative behavior is similar to that of the polarizable model. The barrier heights to dissociation for the bulk and surface cases are the same for this model, in contrast to the polarizable model. The inset shows the invert parabolic fits (red color) to the barrier for the interfacial ion pair.

The computed rate constants from the PMFs shown in Figure 5 using TST (eq 4) were found to be 0.23 and 0.27 ps^{-1} in the bulk and interface, respectively (see Table 2). Comparing these rate constants with the bulk rate constant for the polarizable model of 0.28 ps^{-1} shows a similar, albeit slightly lower, value. This is consistent with what was found for the effect of polarizability on water diffusivity, which found that polarizable models yielded faster dynamics.[24] Of significant interest is the finding that the interface has slightly faster dissociation dynamics than the bulk for the nonpolarizable model, which is in sharp contrast with the polarizable model. For the polarizable model, the rate constant was four times higher in the bulk than that at the interface, which is consistent with the much higher barrier for NaCl dissociation at the interface when compared to the barrier height in the bulk.

The transmission coefficients were computed for the nonpolarizable model in the bulk and at the interface using both the RF method and GH theory. Figure 6 shows transmission coefficients using RF (eq 5) as a function of time in the bulk and at the interface. Both of them approach 0.2, with the bulk and interfacial values nearly identical after 2 ps. The values arrived at these are given in Table 2 and are very close. Again, this is in contrast with the results from use of the polarizable model, which had a much higher transmission coefficient at the interface than in the bulk, indicating a different dissociation mechanism.

The friction kernel calculated via eq 7 as a function of time for the nonpolarizable model in the bulk and at the interface is given in Figure 7. The kernel has much more structure for interfacial NaCl in comparison with the bulk, showing many

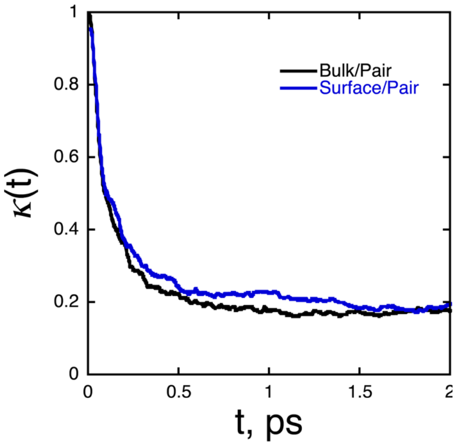

Figure 6. Computed $\kappa(t)$ for the NaCl ion pair in the bulk and at the Gibbs dividing surface. For this potential, the solvent coupling to the reactive motion appears to be the same (nonpolarizable model).

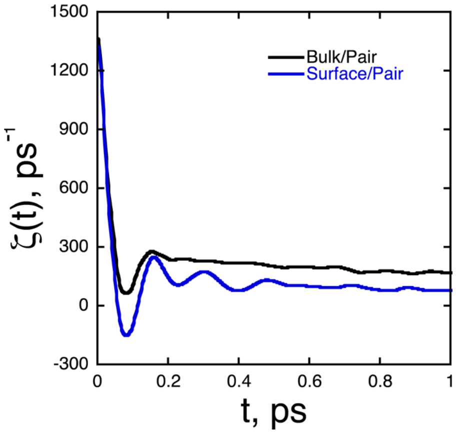

Figure 7. Computed friction kernel, $\zeta(t)$, for the NaCl ion pair in the bulk and at the Gibbs dividing surface. Although the long time scale response is different for the bulk and surface cases, the response that is responsible for the reactive motion is similar. Extra ringing in the surface case corresponds to response that is not coupled to the reactive motion (nonpolarizable model).

Table 3. Dissociation Lifetime: Comparison between Polarizable and Nonpolarizable Models

	τ_{RF}, ps	τ_{GH}, ps
interface/pol	57	43
interface/pair	21	13
bulk/pol	26	20
bulk/pair	26	27

more oscillations at shorter times. This is consistent with how the interface and bulk compared for the polarizable model, except that the nonpolarizable friction kernel at the interface has the most structure of all. Eventually, the kernel at the interface approaches a value that is lower than the value found in the bulk, while the friction kernels for the polarizable models were similar at the interface and bulk. We calculated barrier frequencies, ω_b, of 75.9−79.6 cm^{-1} for the bulk and interfacial ion pairs, respectively. These frequencies are used when calculating the GH transmission coefficients using eq 8. The values determined for the nonpolarizable model at the interface and bulk are given in Table 2. The GH transmission coefficient is higher at the interface than that in the bulk, which is consistent with what we found for the polarizable model. In Table 3, we provide a summary of the dissociation lifetimes of a NaCl pairing using a variety of rate theory approaches and potential models.

Comparing the RF and GH transmission coefficients for both models provides interesting insights. The values for the bulk are consistent between the two theories, showing that GH may be a good approach for understanding kinetics in the bulk. At the interface, however, the GH transmission coefficient is overpredicted in comparison with the RF value by around 0.1 for both polarizable and nonpolarizable models. This suggests that the interface itself adds additional complications that may limit GH theory. A consequence of capillary waves is that even if a molecule is at the Gibbs dividing surface, its local structure fluctuates from a partially solvated (i.e., with fewer water molecules surrounding it) to more fully solvated one. This and potentially other complications provide a challenge in kinetic analyses.

3.C. Generalized Langevin Equation Dynamics. GH theory rate estimates are limited because the barrier is represented by a harmonic approximation and linear response of the solvent is represented by the friction kernel. To understand the consequences of the harmonic approximation, we explore detailed Generalized Langevin Equation (GLE) dynamics associated with this system.[25−27] Given the computed PMFs and the friction kernel, it is instructive to consider the dynamics of the GLE.

$$\mu \frac{d^2}{dt^2} r(t) = -\partial_r W(r) - \mu \int_0^t dt'\, \zeta(t - t') \frac{d}{dt} r(t') + R(t) \tag{9}$$

Corresponding to each of the four cases (i.e., polarizable and nonpolarizable and surface and bulk systems), the friction was fit to the cosine expansion

$$\zeta(t) = \sum_{i=1}^{N} \omega_i^2 c_i^2 \cos(\omega_i t) \tag{10}$$

with a uniform distribution of frequencies, $\omega_j = \frac{\pi}{t_c}(2j - 1)$, $N = 100$, and t_c= 4.838 ps. An effective Hamiltonian can be constructed as follows

$$H = \frac{p_r^2}{2\mu} + W(r) + \sum_{i=1}^{N} \frac{p_{xi}^2}{2\mu} + \frac{1}{2}\mu\omega_i^2(x_i - c_i(r - r^*))^2 \tag{11}$$

by linearly coupling bath coordinates, x_i, and the relative motion through coefficients c_i. It is established that initial conditions drawn from a canonical distribution and canonical dynamics from the Hamiltonian generate an ensemble of classical dynamics that are equivalent to the GLE dynamics for time scales less than the recurrence time, t_c. It is instructive to look at the fitted spectral density represented by $\sum_{i=1}^{N} \omega_i c_i \delta(\omega - \omega_i)$. In Figure 8, we compare the four cases. Here we find extra coupling for the surface systems at higher frequencies (200 cm^{-1}), with reduced coupling at lower frequencies (80 cm^{-1}). The barrier frequency overlaps with the lower-frequency range. Consequently, we expect that the rate process will be less impeded and faster for the surface cases when compared to the bulk. The details of this will be explored by calculating the transmission coefficient and reactive force correlation functions corresponding to GLE dynamics.

DOI: 10.1021/acs.jpcc.7b02223
J. Phys. Chem. C 2017, 121, 10018−10026

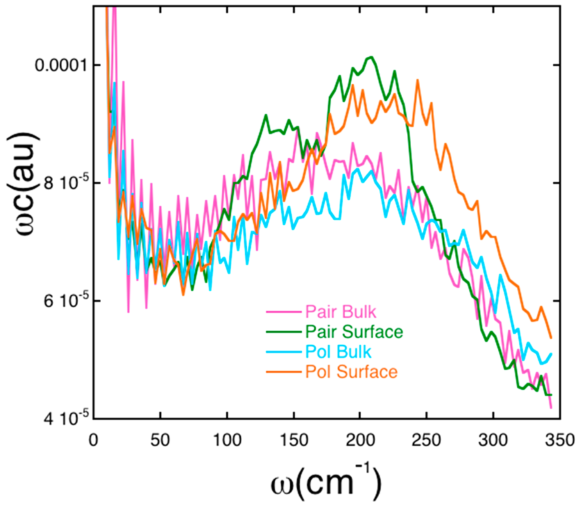

Figure 8. Spectral densities derived from the Fourier transform of the friction kernel, $\zeta(t)$. Notice the additional coupling associated with surface cases at higher frequencies (200 cm^{-1}). In the frequency range that couples to the reactive motion (80 cm^{-1}), the surface cases exhibit smaller coupling and a faster rate constant.

For each of the four cases, we launched dynamics from the dividing surface $r = r^*$ and constructed the reactive force correlation function scaled by the TST rate constant, $\kappa(t)$. These results are labeled as GLE in the curves shown in Figure 9. For comparison, results from the RF simulation are included. For all four cases, the dynamics from the GLE quantitatively recover that from the RF simulation for times less than 0.3 ps. In each of these cases, we plot the GH estimate, κ_{GH}. We find that the GH estimate is in good agreement with $\kappa(t)$ at this point, where short time scale recrossings can be accounted for through rotation of the dividing surface including both degrees of freedom. Any deviations are the result of anharmonic effects. The influence of longer time scale recrossings is not recovered by the GLE dynamics.

As a consistent check, it is possible to launch dynamics from the rotated "GH" surface, the surface where TST is exact (no recrossings for a harmonic system). The resulting $\kappa(t)$ corresponding to this case is labeled by "Rotated Surface GLE" in Figure 9. These results are constant until the transition between short time behavior and long time behavior (~0.3 ps), where additional recrossings take over, becoming consistent with the GLE simulations from the $r = r^*$ dividing surface. (Deviations are associated with anharmonicity.) It appears that the linear coupling represented by GLE dynamics does not quantitatively recover the response of the full system at these longer time scales. It will be the challenge of future work to develop a reduced model, perhaps invoking alternative collective variables (reaction coordinates) that more effectively take into account this longer time scale response.

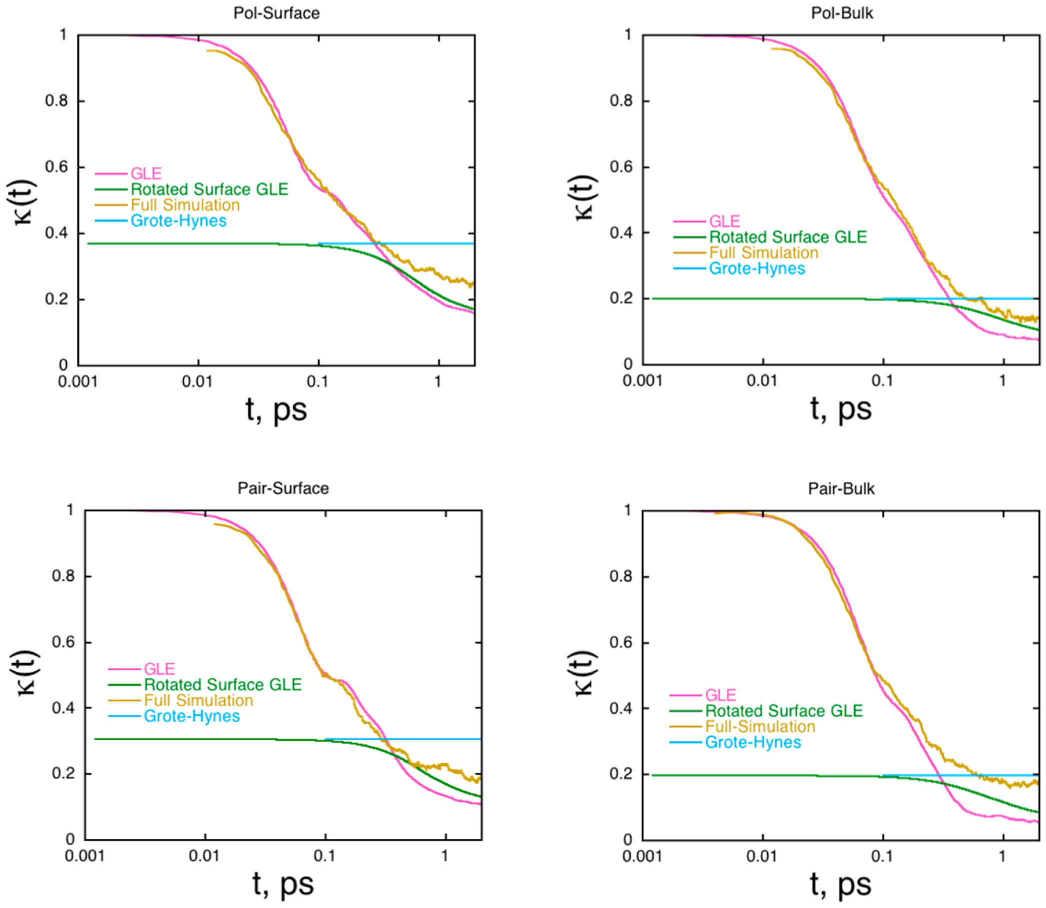

Figure 9. Comparison of the reactive force correlation function for dynamical models. There is complete consistency at short time scales. Linear response and harmonic theories recover the quantitative behavior. Long time GLE behavior is consistent with a rotated dividing surface. GLE dynamics does not completely recover the full simulation response.

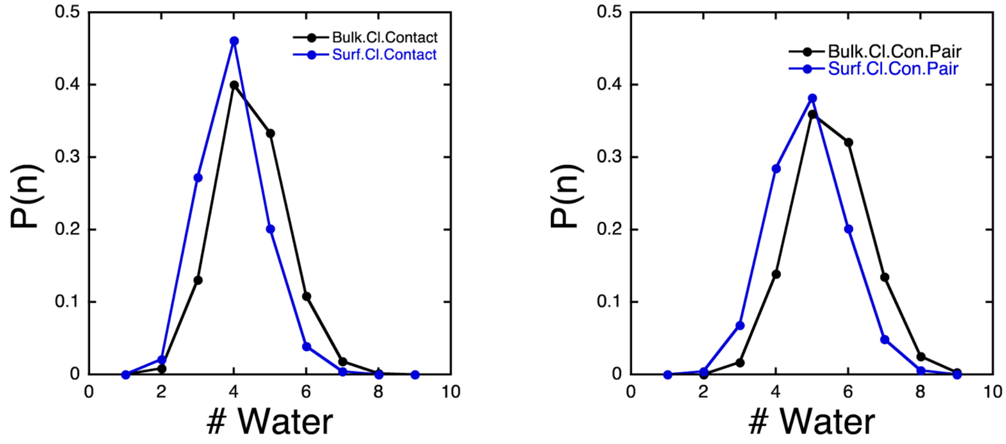

Figure 10. Probability distribution for the number of water molecules around the Cl$^-$ ion while NaCl is at the contact ion pair. The left panel is for the polarizable model, while the right is the nonpolarizable one.

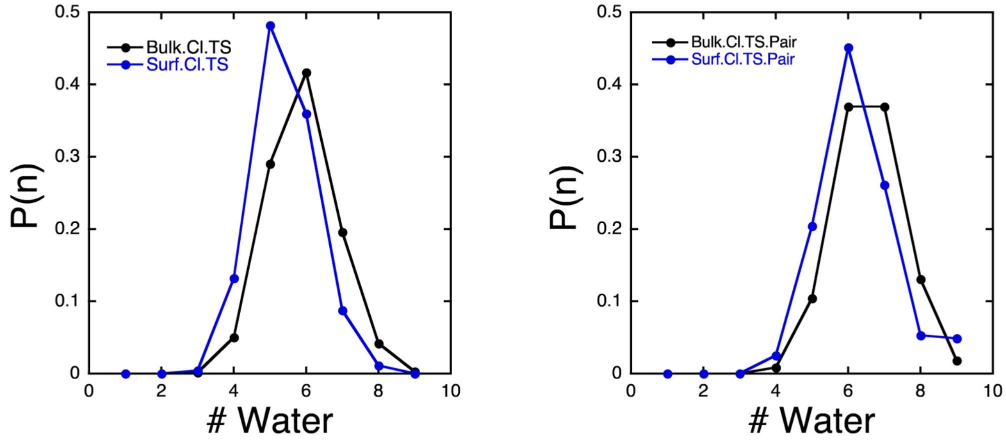

Figure 11. Probability distribution for the number of water molecules around the Cl$^-$ ion while NaCl is at the transition state for dissociation. The left panel is for the polarizable model, while the right is the nonpolarizable one.

3.D. Comparison of Water Structure around Ions. To further understand the differences in the structure of water around the ion pair at the interface and in the bulk, we computed the probability distribution for the number of water molecules around Cl$^-$ for the contact ion pair. This distribution specifically represents the number of water molecules within the first solvation shell of Cl$^-$, defined as when a water oxygen is within 3.7 Å of the Cl$^-$ atom. The results are presented in Figure 10. The first observation is that there is a similar shape to the water distribution around Cl$^-$ in the bulk for both types of models, but more water molecules are surrounding the nonpolarizable model (an average of one more). At the interface, the number of water molecules surrounding each ion is reduced with respect to the bulk. For the nonpolarizable model, the peak width for the distribution appears to be similar at the bulk and interface, with its peak shifted to lower values. For the polarizable model, however, the peak is not only shifted; it is sharper in comparison with the peak in the bulk. This signals a tighter distribution for the number of water molecules surrounding it at the interface.

Figure 11 shows the distribution of water molecules around the Cl$^-$ ion in the bulk and at the interface for the polarizable and nonpolarizable models at the transition state for NaCl dissociation. The number of water molecules surrounding each atom increases with respect to the contact ion pair, with the bulk distribution peaking at six for the polarizable model and ranging from six to seven for the nonpolarizable model. At the interface, both the polarizable and nonpolarizable Cl$^-$ ions have sharper peaks that are shifted lower. It appears that the impact of the interface on the structure surrounding the Cl$^-$ ions is similar for both models. This also is evident when comparing the GH results for the two types of models. The value of κ_{GH} is approximately 1.8 times higher at the interface than that in the bulk for both models, which is consistent with a similar change in water structure near the transition state. However, the RF transmission coefficients in the bulk and at the interface are nearly identical to those for the nonpolarizable model but significantly higher at the interface for the polarizable model. This shows that both the contact ion pair and transition state structure may be important in elucidating the factors that influence ion dissociation.

4. CONCLUSIONS

Despite their importance in many physical phenomena, the impact of interfaces on the kinetics of ion dissociation and pairing, including the impact of polarizable interactions, is not well understood. To address this problem, we carried out a study of the thermodynamics and kinetics of small alkali halide ions in the bulk and near the water vapor−liquid interface. Dissociation rates using classical TST were calculated, and they were weighted with transmission coefficients determined by the RF method and GH theory. We found that ion dissociation is significantly slower at the interface than that in the bulk, but this was only observed with the inclusion of polarizability in the model. Moreover, our results showed that GH theory gave similar results as the RF approach for bulk ion dissociation. However, for interfacial dissociation, GH theory overestimated the transmission coefficient. In general, fewer water molecules were found to be solvated with the Cl^- ion at the interface than in the bulk, and the polarizable model had, on average, one less water molecule within its first solvation shell than the nonpolarizable model. These new findings provide a significant basis for future research using different approaches and techniques. Our future work along this line will include the classical rate theory study of acid dissociation near the water liquid−vapor interface and a comparison of our results with the results of density functional theory-based molecular dynamics simulations by Baer et al.[28]

In addition, we investigated the consequences of a reduced model that simulates the system dynamics, a GLE framework that incorporates the PMF and friction kernel of the full system. In the current work, we explored the dynamics in the ion−ion distance, *r*. In future work, we will extend the analysis to include coordination number dependence as a dynamic variable.[29] This approach represents the solvent coupling to the solute motion through linear coupling determined from linear response, characterized by the force fluctuations of the reactive motion. We found that a majority of short time recrossings are effectively described by such a framework, as well as the harmonic approximation intrinsic to GH theory. This theory overestimates dynamical recrossings, deviations from TST in the motion at longer time scales. Perhaps the solvent coupling near the transition state is too strong compared to that at later stages of dynamics, or perhaps the dominant collective motions differ in nature. These questions will motivate further investigations.

■ AUTHOR INFORMATION

Corresponding Author

*E-mail: liem.dang@pnnl.gov. Phone: 509-302-7924.

ORCID

Liem X. Dang: 0000-0003-4878-2200

Notes

The authors declare no competing financial interest.

■ ACKNOWLEDGMENTS

This work was supported by the U.S. Department of Energy, Office of Science, Office of Basic Energy Sciences, Division of Chemical Sciences, Geosciences, and Biosciences. The calculations were carried out using computer resources provided by the Office of Basic Energy Sciences.

■ REFERENCES

(1) *Biophysics of Water*; Franks, F., Mathias, S., Eds.; Wiley-Interscience: New York, 1982.

(2) McLaughlin, S. The Electrostatic Properties of Membranes. *Annu. Rev. Biophys. Biophys. Chem.* **1989**, *18*, 113.

(3) Honig, B.; Hubbell, W. L.; Flewelling, R. F. Electrostatic Interactions in Membranes and Proteins. *Annu. Rev. Biophys. Biophys. Chem.* **1986**, *15*, 163.

(4) Knipping, E. W.; Lakin, M. J.; Foster, K. L.; Jungwirth, P.; Tobias, D. J.; Gerber, R. B.; Daddub, D.; Finlayson-Pitts, B. Experiments and Simulations of Ion-Enhanced Interfacial Chemistry on Aqueous NaCl Aerosols. *Science* **2000**, *288*, 301 and references therein.

(5) Haag, W. R.; Yao, C. C. D. *Environ. Sci. Technol.* **1992**, *26*, 1005. U.S. Department of Energy, Office of Environmental Management. *FY 1995 Technology Development Needs Summary*; 1994; p 2−17

(6) Schweighofer, K.; Benjamin, I. Ion Pairing and Dissociation at Liquid/Liquid Interfaces: Molecular Dynamics and Continuum Models. *J. Chem. Phys.* **2000**, *112*, 1474−1482.

(7) Venkateshwaran, V.; Vembanur, S.; Garde, S. Water-Mediated Ion−Ion Interactions Are Enhanced at the Water Vapor−Liquid Interface. *Proc. Natl. Acad. Sci. U. S. A.* **2014**, *111*, 8729−8734.

(8) Wick, C. D. NaCl Dissociation Dynamics at the Air-Water Interface. *J. Phys. Chem. C* **2009**, *113*, 2497.

(9) Otten, D. E.; Onorato, R.; Michaels, R.; Goodknight, J.; Saykally, R. J. Strong Surface Adsorption of Aqueous Sodium Nitrite as an Ion Pair. *Chem. Phys. Lett.* **2012**, *519-520*, 45.

(10) Luo, G.; Bu, W.; Mihaylov, M.; Kuzmenko, I.; Schlossman, M. L.; et al. X-ray Reflectivity Reveals a Nonmonotonic Ion-density Profile Perpendicular to the Surface of $ErCl_3$ Aqueous Solutions. *J. Phys. Chem. C* **2013**, *117*, 19082−19090.

(11) Hua, W.; Verreault, D.; Huang, Z.; Adams, E. M.; Allen, H. C. Cation Effects on Interfacial Water Organization of Aqueous Chloride Solutions. I. Monovalent Cations: Li^+, Na^+, K^+, and NH_4^+. *J. Phys. Chem. B* **2014**, *118*, 8433−8440.

(12) Truhlar, D. G.; Hase, W. L.; Hynes, J. T. Current Status of Transition-State Theory. *J. Phys. Chem.* **1983**, *87*, 2664.

(13) Chandler, D. Statistical-Mechanics of Isomerization Dynamics in Liquids and Transition-State Approximation. *J. Chem. Phys.* **1978**, *68*, 2959.

(14) Grote, R. F.; Hynes, J. T. The Stable States Picture of Chemical-Reactions 2. Rate Constants for Condensed and Gas-Phase Reaction Models. *J. Chem. Phys.* **1980**, *73*, 2715.

(15) Dang, L. X.; Chang, T−M. Many-Body Interactions in Liquid Methanol and Its Liquid/Vapor Interface: A Molecular Dynamics Study. *J. Chem. Phys.* **1997**, *106*, 8149.

(16) Dang, L. X. Computational Study of Ion Binding to the Liquid Interface of Water. *J. Phys. Chem. B* **2002**, *106*, 10388−10394.

(17) Guardia, E.; Rey, R.; Padro, J. A. Potential of Mean Force by Constrained Molecular-Dynamics - A Sodium-Chloride Ion-Pair in Water. *Chem. Phys.* **1991**, *155*, 187.

(18) Case, D. A.; Darden, T. A.; Cheatham, T. E., III; Simmerling, C.; Wang, J.; Duke, R. E.; Luo, R.; Merz, K. M.; Pearlman, D. A.; Crowley, M.; et al. *Amber 9*; University of California: San Francisco, CA, 2006.

(19) Berendsen, H. J. C.; Postma, J. P. M.; van Gunsteren, W. F.; DiNola, A.; Haak, J. R. Molecular-Dynamics with Coupling to an External Bath. *J. Chem. Phys.* **1984**, *81*, 3684−3690.

(20) Essmann, U.; Perera, L.; Berkowitz, M. L.; Darden, T.; Lee, H.; Pedersen, L. G. A Smooth Particle Mesh Ewald Method. *J. Chem. Phys.* **1995**, *103*, 8577.

(21) Ryckaert, J. P.; Ciccotti, G.; Berendsen, H. J. C. Numerical-Integration of Cartesian Equations of Motion of a System with Constraints Molecular Dynamics of N-Alkanes. *J. Comput. Phys.* **1977**, *23*, 327.

(22) Wick, C. D.; Kuo, I. F. W.; Mundy, C. J.; Dang, L. X. The Effect of Polarizability for Understanding the Molecular Structure of Aqueous Interfaces. *J. Chem. Theory Comput.* **2007**, *3*, 2002−2010.

(23) Peng, T.; Chang, T.-M.; Sun, X.; Nguyen, A. V.; Dang, L. X. Development of Ions-TIP4P-Ew Force Fields for Molecular Processes in Bulk and at the Aqueous Interface Using Molecular Simulations. *J. Mol. Liq.* **2012**, *173*, 47−54.

(24) Liu, P.; Harder, E.; Berne, B. On the Calculation of Diffusion Coefficients in Confined Fluids and Interfaces with an Application to the Liquid−Vapor Interface of Water. *J. Phys. Chem. B* **2004**, *108*, 6595.

(25) Schenter, G. K.; McRae, R. P.; Garrett, B. C. Dynamic Solvent Effects on Activated Chemical-Reactions 1. Classical Effects of Reaction-Path Curvature. *J. Chem. Phys.* **1992**, *97*, 9116.

(26) McRae, R. P.; Schenter, G. K.; Garrett, B. C. Dynamic Solvent Effects on Activated Chemical Reactions. 2. Quantum Mechanical Effects. *J. Chem. Soc., Faraday Trans.* **1997**, *93*, 997.

DOI: 10.1021/acs.jpcc.7b02223
J. Phys. Chem. C 2017, 121, 10018−10026

(27) Dang, L. X.; Schenter, G. K. Solvent Exchange in Liquid Methanol and Rate Theory. *Chem. Phys. Lett.* **2016**, *643*, 142.

(28) Baer, M.; Tobias, D. J.; Mundy, C. J. Investigation of Interfacial and Bulk Dissociation of HBr, HCl, and HNO_3 Using Density Functional Theory-Based Molecular Dynamics Simulations. *J. Phys. Chem. C* **2014**, *118*, 29412−29420.

(29) Roy, S.; Baer, M. D.; Mundy, C. J.; Schenter, G. K. Reaction Rate Theory in Coordination Number Space: An Application to Ion Solvation. *J. Phys. Chem. C* **2016**, *120*, 7597−7605.

DOI: 10.1021/acs.jpcc.7b02223
J. Phys. Chem. C 2017, 121, 10018−10026